CellPress
Partner Journal

Molecular Plant
Research Report

Structure-guided analysis of *Arabidopsis* JASMONATE-INDUCED OXYGENASE (JOX) 2 reveals key residues for recognition of jasmonic acid substrate by plant JOXs

Xin Zhang[1,4], Dongli Wang[1,4], Joyce Elberse[2], Linlu Qi[1], Wei Shi[1], You-Liang Peng[1], Robert C. Schuurink[3], Guido Van den Ackerveken[2,*] and Junfeng Liu[1,*]

[1]State Key Laboratory of Agrobiotechnology, Ministry of Agriculture Key Laboratory for Crop Pest Monitoring and Green Control, Joint International Research Laboratory of Crop Molecular Breeding, College of Plant Protection, China Agricultural University, Beijing 100193, China

[2]Plant-Microbe Interactions, Department of Biology, Utrecht University, 3508 TB Utrecht, the Netherlands

[3]Green Life Sciences Research Cluster, Swammerdam Institute for Life Sciences, University of Amsterdam, 1098 XH Amsterdam, the Netherlands

[4]These authors contributed equally to this article.

***Correspondence: Guido Van den Ackerveken (g.vandenackerveken@uu.nl), Junfeng Liu (jliu@cau.edu.cn)**

https://doi.org/10.1016/j.molp.2021.01.017

ABSTRACT

The jasmonic acid (JA) signaling pathway is used by plants to control wound responses. The persistent accumulation of JA inhibits plant growth, and the hydroxylation of JA to 12-hydroxy-JA by JASMONATE-INDUCED OXYGENASEs (JOXs, also named jasmonic acid oxidases) is therefore vital for plant growth, while structural details of JA recognition by JOXs are unknown. Here, we present the 2.65 Å resolution X-ray crystal structure of *Arabidopsis* JOX2 in complex with its substrate JA and its co-substrates 2-oxoglutarate and Fe(II). JOX2 contains a distorted double-stranded β helix (DSBH) core flanked by α helices and loops. JA is bound in the narrow substrate pocket by hydrogen bonds with the arginine triad R225, R350, and R354 and by hydrophobic interactions mainly with the phenylalanine triad F157, F317, and F346. The most critical residues for JA binding are F157 and R225, both from the DSBH core, which interact with the cyclopentane ring of JA. The spatial distribution of critical residues for JA binding and the shape of the substrate-binding pocket together define the substrate selectivity of the JOXs. Sequence alignment shows that these critical residues are conserved among JOXs from higher plants. Collectively, our study provides insights into the mechanism by which higher plants hydroxylate the hormone JA.

Key words: crystal structure, JASMONATE-INDUCED OXYGENASEs (JOXs), jasmonic acid (JA), 12-OH-JA, hydroxylation

Zhang X., Wang D., Elberse J., Qi L., Shi W., Peng Y.-L., Schuurink R.C., Van den Ackerveken G., and Liu J. (2021). Structure-guided analysis of *Arabidopsis* JASMONATE-INDUCED OXYGENASE (JOX) 2 reveals key residues for recognition of jasmonic acid substrate by plant JOXs. Mol. Plant. **14**, 820–828.

INTRODUCTION

Jasmonates are phytohormones that are especially important in the response to wounding, herbivore damage, and necrotrophic pathogens (Wasternack and Strnad, 2016). In plants, jasmonates exist as derivatives that can be biologically active, inactive, or have reduced activity (Wasternack and Strnad, 2016). The most active jasmonate is jasmonic acid-isoleucine (JA-Ile), the Ile conjugate of JA (Fonseca et al., 2009). Upon wounding or herbivore attack, JA-Ile is produced and is sensed by the COI (coronatine-insensitive 1) receptor complex, which then promotes the degradation of JAZ (jasmonate ZIM domain) proteins, resulting in the de-repression of JA-regulated genes, e.g., *PDF1.2* (Xie et al., 1998; Devoto et al., 2002; Thines et al., 2007; Katsir et al., 2008; Fernandez-Calvo et al., 2011; Niu et al., 2011; Zhu et al., 2011; Yan et al., 2018). However, the accumulation of JA and JA-Ile can inhibit plant growth (Huot et al., 2014). Plants regulate the levels of JA and JA-Ile by

Published by the Molecular Plant Shanghai Editorial Office in association with Cell Press, an imprint of Elsevier Inc., on behalf of CSPB and CEMPS, CAS.

converting them to the biologically inactive forms 12-OH-JA and 12-OH-JA-Ile, respectively (Wasternack and Strnad, 2016).

In 2017, four JASMONATE-INDUCED OXYGENASEs (JOXs, JOX1–4, also named jasmonic acid oxidases [JAOs]) were found to catalyze the hydroxylation of JA to 12-OH-JA in the model plant *Arabidopsis thaliana* (Figure 1A) (Caarls et al., 2017; Smirnova et al., 2017). An *Arabidopsis* quadruple *jox* mutant, *joxQ*, displayed reduced growth, constitutively elevated JA and JA-Ile levels, and enhanced defense against insects and fungi (Caarls et al., 2017). The oxidation of JA to 12-OH-JA can be considered a metabolic shunt that diverts JA from conversion to JA-Ile, the biologically active form of jasmonate (Smirnova et al., 2017). The JOXs form a single paralogous family, clade 46 of dioxygenase class C (DOXC) of the 2-oxoglutarate (2OG)-dependent oxygenase superfamily in *Arabidopsis* (Kawai et al., 2014). Plant 2OG-dependent oxygenases have been classified into three classes, DOXA (dioxygenases A, homologs of *Escherichia coli* AlkB, a DNA repair protein that responds to alkylating agents), DOXB (dioxygenases B, which contain a prolyl 4-hydroxylase domain), and DOXC (Kawai et al., 2014). DOXC is the largest and most functionally diverse class of plant 2OG-dependent oxygenases that act in the metabolism of phytohormones such as ethylene, gibberellins, auxin, and salicylic acid (Kawai et al., 2014). Because the genetic removal of only *JOX2* is sufficient to increase JA-Ile signaling and resistance to attackers, we chose JOX2 for crystallography and related assays (Smirnova et al., 2017). Here, we report the three-dimensional structure of *Arabidopsis* JOX2 in complex with the substrate JA and the co-substrates 2OG and iron, revealing critical residues for substrate binding and hydroxylation.

RESULTS AND DISCUSSION

Overall structure

We obtained homogeneous recombinant full-length JOX2 protein (residues 1–371) from *E. coli* (Supplemental Figure 1A and 1B). Inductively coupled plasma mass spectrometry (ICP–MS) showed that 65.5% of the protein contained iron, whereas 18.2% contained zinc instead of iron owing to the expression of this metalloenzyme in *E. coli*. Crystallization was not successful until JA was added to the protein solution, suggesting that JA stabilized the conformation of JOX2 for crystal packing. Size-exclusion chromatography of JOX2 supplemented with JA indicated that JOX2 was a monomer in solution, and crystal packing of one asymmetric unit showed that two protein molecules formed a symmetry-mate dimer (Supplemental Figure 1A and 1C). The structure was determined at 2.65 Å (Supplemental Table 1). Residues D18–P50, A59–L70, and D78–P370 of JOX2 were built into the model; other residues were not because their electron density was not detected owing to flexibility or disorder (Figure 1B). Extra electron density inside JOX2 was observed and provided positional information for a 2OG, an iron atom, and a JA substrate (Supplemental Figure 2). JA adopts the *trans* form (with respect to the cyclopentane ring) (3R,7R)-JA, which is more stable than the *cis* form (3R,7S)-JA (Supplemental Figure 2).

The JOX2 molecule contains an N-terminal region (residues M1–E218), a distorted double-stranded β helix (DSBH) core (residues N219–P320), and a small C-terminal region (residues K321–R371) (Figure 1B and Supplemental Figure 3). The N-terminal region contains six α helices (α1–α6) and four β strands (βN1–βN4). The DSBH core has eight conserved β strands (βI–βVIII) and a short α helix (α7) between the βVI and βVII strands. It should be noted that, although the βII strand (residues L241–D246) appears as a loop in the structural model, a Ramachandran plot of its residues shows that they all fall into the β strand region (Supplemental Figure 4). The C-terminal region contains two α helices, α8 and α9 (Figure 1B and Supplemental Figure 3). The iron and 2OG reside in the DSBH core, whereas the JA lies in a region surrounded by both the DSBH core and the N- and C-terminal regions (Figure 1B). The DSBH core and the positioning of 2OG, Fe, and substrate are conserved among 2OG-dependent oxygenases (Supplemental Figure 5A and 5B). In JOX2, the distance between the iron and the C12 carbon atom of JA, which is proposed to undergo the oxygenation reaction, is 4.4 Å, which is consistent with oxidation via initial hydrogen atom abstraction followed by rapid hydroxylation (Supplemental Figure 2) (Aik et al., 2015).

Analysis of the active site of JOX2

The active site of JOX2 consists of 2OG, iron, and critical residues that interact with them (Figure 2A). The 2OG is bound by residues from the DSBH core through hydrogen bonds and hydrophobic interactions. Hydrogen bonds are formed between the C5 carboxyl group of 2OG and the side-chain amino or hydroxyl groups of residues Y229, R311, and S313 (Figure 2A). The non-polar residues L241, L253, L262, V303, and A315 interact with carbon atoms of 2OG through hydrophobic interactions. The iron atom is coordinated by the conserved residues His-X-Asp/Glu…His, also called the facial triad (Figure 2A) (Hausinger, 2015). The coordination number of iron is six, three of which come from the side-chain nitrogen or oxygen atoms of the facial triad, i.e., residues H244, D246, and H301 in JOX2. The other three coordination sites come from the two oxygen atoms of the C1 carboxyl group and one oxygen atom of the ketone group of 2OG. Analysis of reported 2OG-dependent oxygenase structures, e.g., VioC (PDB: 6ALM), suggests that the C1 carboxyl group of 2OG must rearrange its position *cis* to the distal His (H244 of JOX2) to allow dioxygen binding (i.e., 2OG provides two coordination sites for iron). This rearrangement may be one of the rate-limiting steps in the catalytic reaction of 2OG oxygenases (Supplemental Figure 6) (Yang et al., 2008; Aik et al., 2015; Mitchell et al., 2017). In the JOX2 structure, the C1 carboxyl group of 2OG is not *cis* to H301 (Figure 2A). An additional hydrogen bond is observed between one oxygen atom of the C1 carboxyl group of 2OG and a side-chain nitrogen of residue N227, which influences the position of the C1 carboxyl group of 2OG (Figure 2A). The hydroxylation reaction did not occur in the crystal because no reducing reagent was added to the protein and well buffer.

Factors that determine the substrate selectivity of JOX2

Two factors determine the substrate selectivity of JOX2, one of which is the shape of its substrate pocket (Figure 2B). The substrate pocket of JOX2 is long and narrow and is occupied by 2OG and JA. The shape of the pocket suggests that JA binding occurs after that of 2OG (because JA binding occludes access to the 2OG binding pocket) and that after the reaction, the 12-OH-JA product may be released before the succinate. It is likely that the binding of 2OG and iron influence the binding of the JA

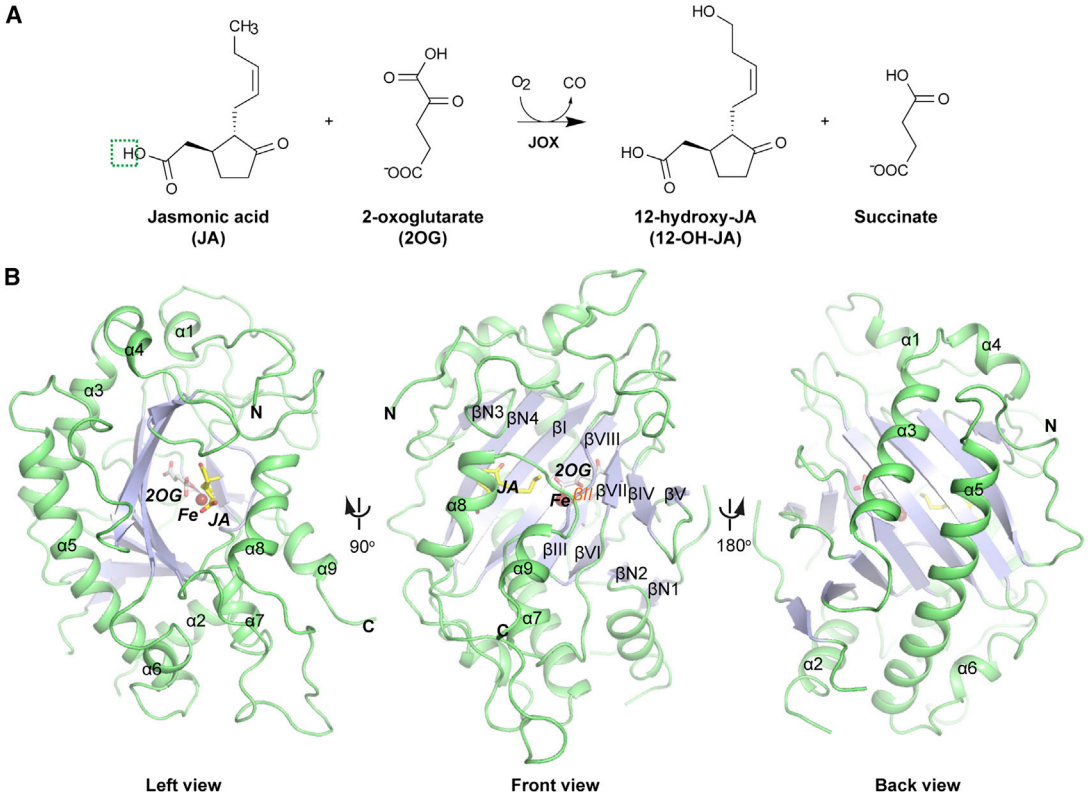

Figure 1. The hydroxylation reaction catalyzed by JOX and the overall structure of the JOX2 complex.
(A) The hydroxylation reaction catalyzed by JOX. The green dashed box indicates the atoms that are different from MeJA and JA-Ile.
(B) Overall structure of the JOX2 complex: left, front, and back views. The β strands are colored light blue, and the α helices and loops are colored lime green. Numbering of β strands and α helices is labeled. 2OG and JA are shown as sticks, and oxygen atoms are colored red. Iron is shown as brown spheres. "N" and "C" indicate the N and C termini of JOX2, if visible, in the respective views.

substrate, as NMR studies on AlkB have revealed that the binding of 2OG and Fe(II) substantially stabilizes the structure of the substrate pocket (Bleijlevens et al., 2008; Ergel et al., 2014). JA and its derivatives differ in the atoms conjugated to the carboxyl group of JA (Figures 1A and 2C). It seems that the substrate pocket of JOX2 cannot accommodate other JA derivatives such as methyl jasmonate (MeJA) and JA-Ile (Figures 1A, 2B, and 2C). Isothermal titration calorimetry (ITC) did not detect the binding of MeJA or JA-Ile by JOX2, whereas the binding affinity between JA and JOX2 was approximately 8.47 μM, suggesting that the binding affinity between JA and JOX2 is higher than that of the other two JA derivatives (Figure 2D and Supplemental Figure 7). Furthermore, we used high-performance liquid chromatography–mass spectrometry (HPLC–MS) to analyze the reaction product of JOX2 after supplementation with JA, MeJA, or JA-Ile. 12-OH-JA was detected when JOX2 was supplemented with JA, but 12-OH-MeJA or 12-OH-JA-Ile were not detected in the other two reaction samples (Supplemental Figure 8).

The residues for substrate binding are the second factor that determines the substrate selectivity of JOX2 (Figure 3A). In the substrate binding site of JOX2, critical residues for JA interaction are found in the N-terminal region (α4–βN3 loop, βN3–βN4 loop, and βN4 strand), the DSBH core (βI strand, βII strand, βII–βIII loop, and βVIII strand), and the C-terminal region (α8 helix) (Figure 3A and Supplemental Figure 3). The critical residues that interact with JA can be classified according to their residue properties. Residue H244 is a member of the facial triad. It uses its side-chain carbon atoms to form hydrophobic interactions with the C10–C12 carbon atoms of JA. The positively charged residues R225, R350, and R354, named the arginine triad here, are involved in hydrogen bonding with JA. Residue R225 uses its primary amino group nitrogen to interact with the ketone oxygen of the JA cyclopentane, whereas residues R350 and R354 form hydrogen bonds with their side-chain nitrogen atoms to the JA carboxyl group. The three phenylalanine residues F157, F317, and F346, named the phenylalanine triad here, use their side chains to form hydrophobic interactions with JA carbon atoms. In particular, the benzene ring of residue F157 is parallel to the JA cyclopentane ring, thereby stabilizing the position of the substrate in a manner similar to π-stacking between benzene rings. Additional residues form hydrophobic interactions with JA, including Y135, L142, L241, P247, and I353. In summary, the position of JA is strictly bound by six hydrogen bonds and one π-stacking residue, F157. It has been reported that precise positioning of the substrate is indispensable for achieving selective oxidation of the correct substrate atoms and avoiding self-oxidation of the 2OG oxygenase itself (Liu et al., 2001; Ryle and Hausinger, 2002; Mantri et al., 2012).

Evaluation of the critical residues

We designed substitutions of JOX2 residues critical for the JA interaction in order to evaluate our structural model and

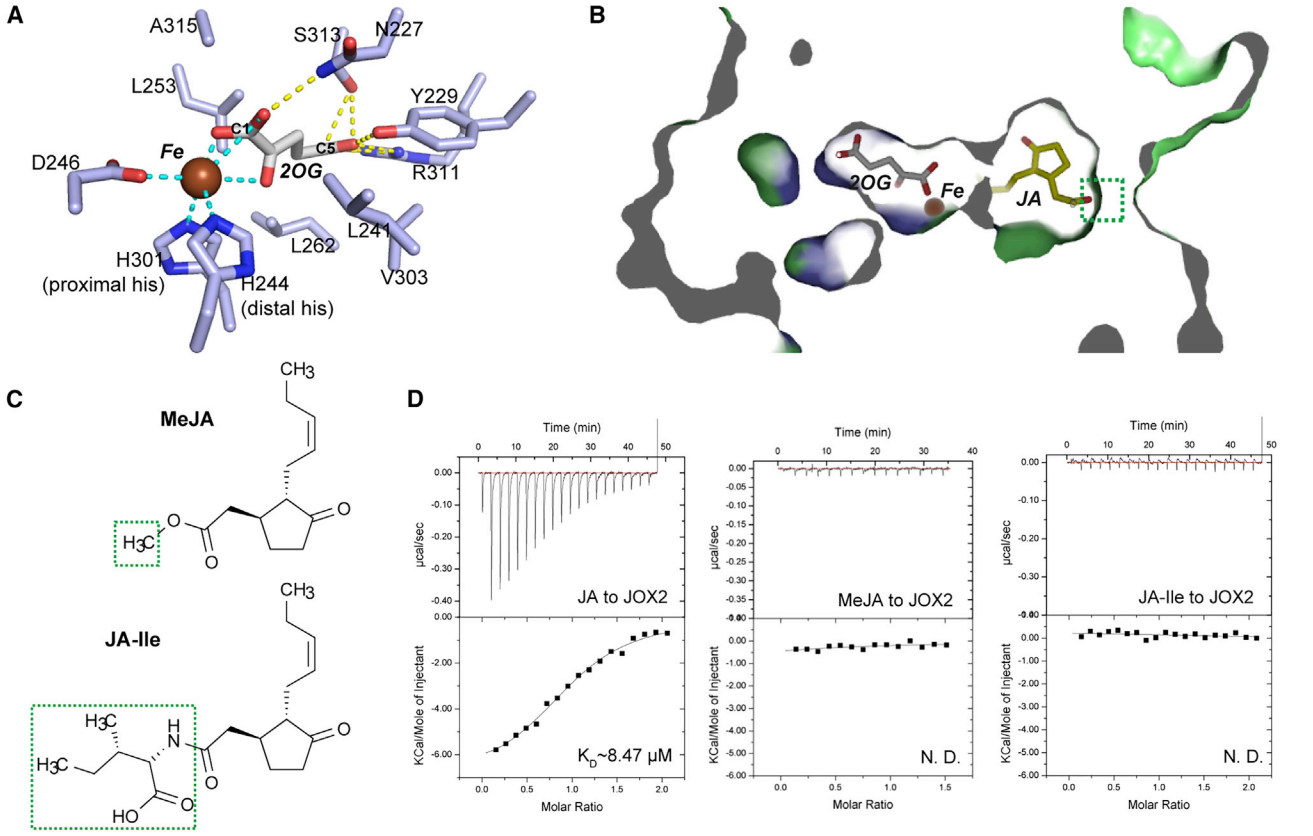

Figure 2. Active site and substrate pocket of JOX2.

(A) Active site of JOX2. Yellow and cyan dashed lines denote hydrogen bonds (<3.5 Å) and coordinations with iron (<3.5 Å), respectively. The iron atom is shown as a brown sphere. 2OG and critical residues are shown as sticks and colored by atom type: red for oxygen and blue for nitrogen. The C1 and C5 carbon atoms of 2OG are labeled. All the critical residues belong to β strands of the DSBH core, and their carbon atoms are colored light blue as in Figure 1B.

(B) Sectional view of the JOX2 substrate pocket. JOX2 is colored as described in Figure 1B. The iron is shown as a sphere. JA and 2OG are shown as sticks with oxygen atoms colored red.

(C) Chemical formula of MeJA and JA-Ile. In **(B)** and **(C)**, the green dashed boxes indicate the atoms that differ among the jasmonates (please refer to Figure 1A for the chemical formula of JA).

(D) ITC experiment results show the binding profiles of JA, MeJA, and JA-Ile to JOX2. The concentrations used were 500 μM for ligands and 50 μM for JOX2 protein. Parameters are shown in the Supplemental figures.

functional predictions. We also included residue D246, which does not interact with JA but is a member of the facial triad. Mutant proteins were purified from *E. coli*, and far-UV circular dichroism (CD) spectroscopy assays showed that the recombinant proteins were well structured, similar to the wild-type (WT) JOX2 protein (Supplemental Figures 1B and 9). *In vitro* binding assays with ITC revealed that the binding affinity of JOX2 for JA was about 8.47 μM, whereas the binding affinity of JA to mutant proteins reached the measurement limit of ITC (Supplemental Figure 7A). Although weak heat changes could be detected with R350A, R354A, and F317A mutants, the results could not be calculated precisely (Supplemental Figure 7B). We also tried a fluorescence-based method to determine the K_m and V_{max} values of JOX2 WT and mutant proteins. Although both the K_m and V_{max} values of the mutants decreased compared with the WT, the results from four mutants (H244A, R225A, F157A, and Y135A) were low and erratic and could not be properly fitted to the Michaelis–Menten function (Supplemental Figure 10). Therefore, we turned to the investigation of *in vitro* enzyme activity and *in planta* effects of the mutant proteins in order to evaluate the roles of the critical residues (Figures 3B and 4A–4D and Supplemental Figure 11).

The enzyme activity of the recombinant proteins, determined by measuring the production of 12-OH-JA from JA, showed a complete loss-of-function in the H244A, R225A, and F157A mutants (Figure 3B). Overexpression of the corresponding mutant genes in the *Arabidopsis joxQ* mutant also did not restore the growth phenotype (Figure 4A and 4B and Supplemental Figure 11A) or reduce expression of the JA marker gene *PDF1.2* (Figure 4C) and JA/JA-Ile levels (Figure 4D and Supplemental Figure 11B), which are high in *joxQ*. By contrast, overexpression of the WT JOX2 fully restored growth and lowered *PDF1.2* expression and JA/JA-Ile accumulation (Figure 4A–4D and Supplemental Figure 11B). These data indicate that residues R225 and F157, both of which are involved in the stabilization of the JA cyclopentane ring, indeed play crucial roles in the activity of the JOX2 enzyme (Figure 3A). Also, overexpression of the

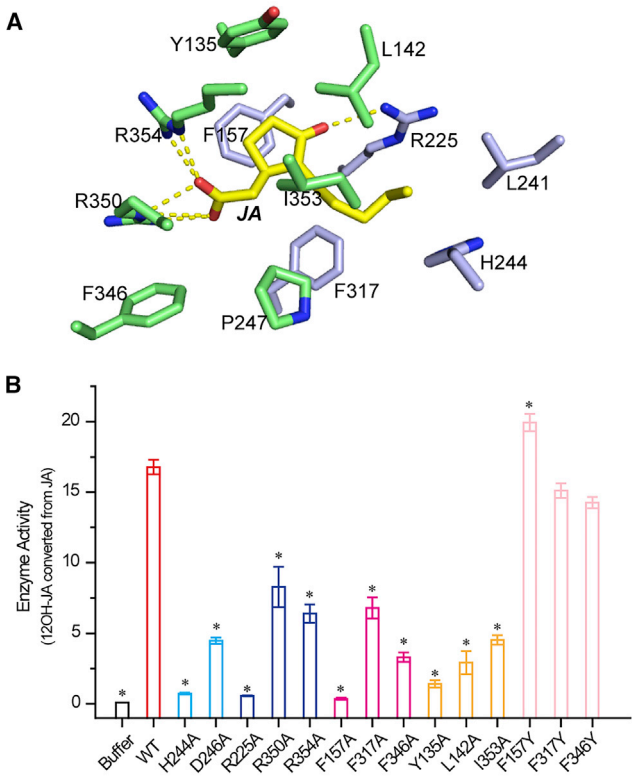

Figure 3. Substrate binding site of JOX2 and *in vitro* evaluation of critical residues for JA interaction.

(A) Substrate binding site of JOX2. The JA and critical residues are shown as sticks and colored by atom type: red for oxygen and blue for nitrogen. Carbon atoms of the critical residues are colored as in Figure 1B. Yellow dashed lines denote hydrogen bonds (<3.5 Å).

(B) Enzyme activity of JOX2 and its mutants determined by their ability to convert JA to 12-OH-JA. The relative enzyme activity was determined by dividing the area of 12-OH-JA by the area of 10 ng IAA, which was added to each sample as an internal reference. Data are presented as mean ± SEM (standard error of the mean). The samples are colored according to the properties of the residues: cyan for the facial triad, blue for the arginine triad, pink for the phenylalanine triad, orange for other hydrophobic residues, and light pink for phenylalanine mutated to tyrosine. Statistical analysis was performed by one-way ANOVA with Tukey's correction for multiple comparisons, significance was defined using $p < 0.05$, and those significantly different from the WT are labeled with an asterisk.

D246A-encoding gene in the *joxQ* mutant did not complement plant growth or *PDF1.2* expression and JA/JA-Ile levels, although the recombinant D246A protein retained ~26.7% of its enzymatic activity *in vitro* (Figures 3B and 4A–4D and Supplemental Figure 11A and 11B). The role of residue D246 is to coordinate the iron atom with residues H244 and H301 and with 2OG. D246 is at the opposite side of 2OG and the H244 and H301 residues (Figure 2A); it is therefore probable that the coordination of iron without D246 can initiate the reaction to some extent when both iron and 2OG are sufficient in the *in vitro* enzyme assay (Figure 3B). Seven other substitutions, R350A, R354A, F317A, F346A, Y135A, L142A, and I353A, all resulted in proteins with reduced enzyme activity (Figure 3B). Similarly, overexpression of the corresponding mutant genes also partially complemented the growth phenotype, *PDF1.2* expression, and JA degradation (Figure 4A–4D and Supplemental Figure 11A and 11B). Therefore, we conclude that residues F157 and R225 are crucial for binding the JA substrate. Substitution of residues F157, F317, and F346 with tyrosine did not affect JOX2 complementation of the *Arabidopsis joxQ* mutant (Figure 4A–4D and Supplemental Figure 11A and 11B). This confirms that the aromatic rings of the three phenylalanine residues, especially F157, are crucial for positioning JA, as they can be substituted with tyrosine but not with alanine (Figure 3A and Supplemental Figure 3).

Critical residues are conserved in plants that contain JOXs

The four *Arabidopsis* JOXs belong to clade 46 of the DOXC class, which was defined by Kawai et al. (2014) based on phylogenetic analysis of 2OG oxygenases from six representative plants species: *Chlamydomonas reinhardtii* (Chlorophyta, green alga), *Physcomitrella patens* (Bryophyta, moss), *Selaginella moellendorffii* (Pteridophyta, club-moss), *Arabidopsis* (Angiospermae), *Oryza sativa* (Angiospermae, rice), and *Picea abies* (Gymnospermae, Norway spruce) (Kawai et al., 2014). Members of clade 47, the clade most closely adjacent to clade 46, are anthocyanidin or flavonol synthases, and we therefore speculate that only the clade 46 members are JOXs (Kawai et al., 2014). Clade 46 contains 17 genes, four from *Arabidopsis*, four from *O. sativa*, and nine from *P. abies*. Sequence alignment of JOXs from clade 46 shows that all the critical residues for JA interaction are conserved, especially the arginine triad R225, R350, and R354, indicating their importance for JA substrate binding (Supplemental Figure 3). The other two critical residues F157 and F346 are tyrosines in JOX1 and JOX3; this substitution did not influence the enzyme activity of JOX2 (Figures 3B and 4A–4D and Supplemental Figures 3 and 11B).

To explore how JOXs evolved a JA preference, we selected two other DOXC enzymes whose structures have been solved: AtLDOX (*Arabidopsis* leucoanthocyanidin dioxygenase, i.e., anthocyanin synthase) from clade 47 and DmH6H (*Datura metel* hyoscyamine 6-hydroxylase) from clade 41 (Supplemental Figure 5) (Wilmouth et al., 2002; Kluza et al., 2020). Structural comparison shows that they share similar secondary structural features with JOX2 (Supplemental Figure 5A). Structural superimposition shows that the positions of 2OG, Fe/Ni, and substrates are similar with respect to the DSBH cores (Supplemental Figure 5B). Their sequence alignment with clade 46 shows that the facial triad for iron interaction and residues Y229, R311, and S313 that form the hydrogen bond with 2OG are strictly conserved, supporting their conserved 2OG-Fe-dependent oxygenase activity. The arginine triad of JOXs contains the most conserved critical residues for JA binding, indicating that hydrogen bonds formed between the arginine triad and JA are the most important feature for substrate determination (Supplemental Figure 3).

Although JA is essential for plant defense, the persistent accumulation of JA hampers plant growth. The JOXs are responsible for the metabolic shunt of JA to 12-OH-JA, thereby playing vital roles in the balance between defense and growth of plants. In this study, we explained the two factors that determine the substrate specificity of *Arabidopsis* JOX2: the shape of the substrate pocket that rejects other jasmonates, and the critical residues,

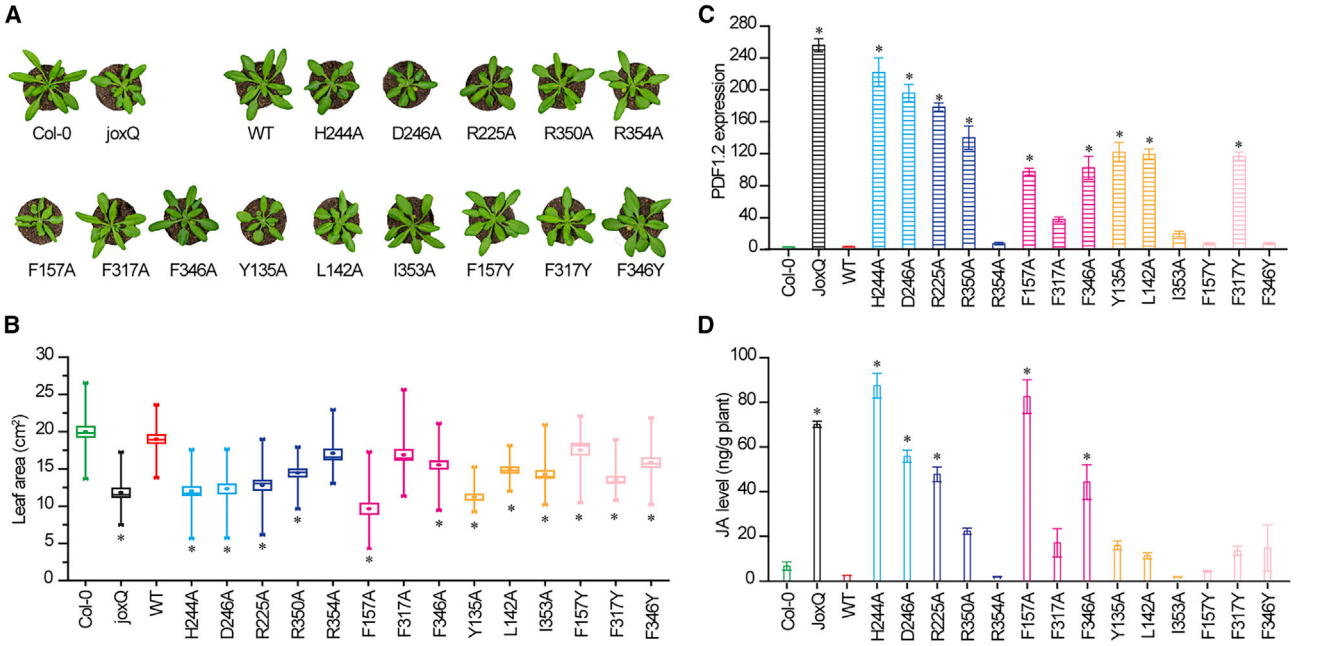

Figure 4. *In planta* analysis of critical residues in JOX2.

(A) Growth phenotype of representative plants of Col-0, *joxQ*, and overexpression lines of *JOX2* (WT and mutants) in the *joxQ* background. Col-0, wild-type *Arabidopsis*; *JoxQ*, the *jox1 jox2 jox3 jox4* quadruple mutant of Col-0.

(B) Growth of plants in **(A)** shown with a box chart. Each data point represents the mean (shown with solid dots inside the boxes) of 24 biological replicates. Box range indicates the SE.

(C) *PDF1.2* gene expression in the plants in **(A)**.

(D) JA accumulation in the plants in **(A)**.

In **(C)** and **(D)**, each data point represents the mean of four biological replicates; error bars indicate the SE. In **(B)**–**(D)**, the data are colored according to the residue properties: cyan for the facial triad, blue for the arginine triad, pink for the phenylalanine triad, orange for other hydrophobic residues, and light pink for phenylalanine mutated to tyrosine. Statistical analysis was performed by one-way ANOVA with Tukey's correction for multiple comparisons, significance was defined using $p < 0.05$, and genotypes that differed significantly from the WT are labeled with an asterisk.

especially the conserved arginine triad and phenylalanine triad, which reject other non-jasmonate phytohormones. In conclusion, our study provides a universal interpretation of how plant JOXs recognize their JA substrate for hydroxylation.

METHODS

Protein expression and purification

The *JOX2* gene (Genbank: NM_120642) was codon-optimized and expressed using a pHAT2 vector (Peranen et al., 1996) with an N-terminal 6× His tag in *E. coli* BL21 (DE3) strain. Protein expression was induced by the addition of 0.2 mM isopropyl-β-D-thiogalactopyranoside to log-phase cultures (optical density at 600 nm of 0.6) grown in LB medium supplemented with 50 μg/ml ampicillin with shaking at 16°C for 16 h. Cells were harvested by centrifugation and lysed by sonication with lysis buffer (20 mM Tris–HCl, 150 mM NaCl, 20 mM imidazole [pH 7.5]). Recombinant protein was collected from Nickel-Chelating Sepharose Fast Flow columns (GE Healthcare) using elution buffer (20 mM Tris–HCl, 150 mM NaCl, 300 mM imidazole [pH 7.5]) and further purified by gel filtration chromatography with a Superdex 200 10/300 gel filtration column (GE Healthcare) equilibrated with storage buffer (20 mM Tris–HCl, 150 mM NaCl [pH 8.0]). The JOX2 mutant proteins were expressed and purified with the same procedure.

Crystallization

WT JOX2 protein was concentrated to ~10 mg/ml (determined with A_{280}, extinction coefficient 52, 495, i.e., absorbance 0.1% [=1 mg/ml] equals A_{280} of 1.221) and supplemented with 5 mM JA (Sigma-Aldrich) for crystallization. Crystallization was performed at 18°C using a sitting-drop diffusion method with an Oryx4 robot (Douglas Instruments). Each drop contained 0.25 μl protein and 0.25 μl reservoir solution equilibrated against a 35 μl reservoir solution. Crystals for data collection were obtained from reservoir solution containing 0.1 M HEPES (pH 7.5) and 1.26 M ammonium sulfate. Crystals were fast-frozen in liquid nitrogen and stored for data collection.

Data collection and structure determination

Diffraction data were collected at the Shanghai Synchrotron Radiation facility BL18U1 beamline. Data were indexed, integrated, and scaled with HKL-2000 (Otwinowski and Minor, 1997). The initial phase was obtained by molecular replacement using Phaser MR of the CCP4 software suite (Potterton et al., 2003) and the *A. thaliana* anthocyanidin synthase structure (PDB: 1GP4; sequence identity, 33.0%) as a search model (Wilmouth et al., 2002). The phase was optimized by interactive model correction with COOT (Emsley and Cowtan, 2004) and refinement with PHENIX (Adams et al., 2010) until the R_{work} and R_{free} values converged. The final model was validated with MolProbity (Chen et al., 2010). Data processing and refinement statistics are listed in Supplemental Table 1. All structure figures were created using PyMOL (DeLano, 2002).

ICP–MS

A JOX2 protein sample (26.21 mg/ml with a theoretical iron concentration of 34.04 ppm [parts per million] [w/w] if each protein contains one iron atom) was prepared in storage buffer. Protein sample (0.5 ml) and 3 ml

HNO_3 were added to a 10 ml PTFE tube, treated on an electric hot plate at 180°C until no obvious reaction was observed and the volume was <2 ml, removed from the plate, cooled, and supplemented with ddH_2O to 10 ml. The solution was analyzed on an iCAP Q instrument (Thermo Scientific). The calculated results were 22.282 ppm for iron and 6.206 ppm for zinc.

Enzyme activity assay with HPLC–MS

JOX2 WT and mutant proteins were prepared in storage buffer. JA, MeJA, JA-Ile, and indole-3-acetic acid (IAA) (all from Sigma) were dissolved in methanol. Each reaction sample contained 10 μg protein, 20 μM JA (or MeJA/JA-Ile), 2 mM α-ketoglutaric acid (2OG) (Sigma), 1 mM $FeSO_4$, 5 mM sodium L-ascorbate (Sigma), 5 mM DTT, and 10 ng IAA (as an internal reference) and was adjusted to 100 μl with storage buffer. The mixture was incubated at 30°C for 2 h for the hydroxylation reaction and then preserved on ice. HPLC–MS was used to quantify jasmonates in each reaction mixture. The samples were separated using an Agilent 1260 Infinity HPLC system coupled online with an Agilent 6520 Q-TOF mass spectrometer equipped with an ESI ion source. The analytical column was an Agilent Extend-C18 column (2.1 × 100 mm, 3.5 mm). Isocratic elution was used with 80% (v/v) acetonitrile plus 0.1% (v/v) formic acid at a flow rate of 0.3 ml/min. The MS parameters were: negative mode, gas temperature 345°C, drying gas flow 11 l/min, VCap 3.5 kV, and full scan mass range m/z 100–1200. The qualitative analysis of MS data was performed using MassHunter software. The values of relative enzyme activity were determined by dividing the area of 12-OH-JA by the area of 10 ng IAA supplemented in each measured sample.

CD

JOX2 WT and mutant proteins were prepared in 20 mM PBS buffer and adjusted to 0.2 mg/ml. CD spectra were recorded on a Chirascan Plus spectropolarimeter (Applied Photophysics) at room temperature with a 0.1-cm path length quartz cuvette. Data were recorded between 190 and 260 nm at a scanning speed of 60 nm/min. Each scan was obtained by recording data points every 0.5 nm with a bandwidth of 2 nm and an integration time of 1 s. Final spectra were the average of three scans and were corrected by subtracting a spectrum of the PBS buffer recorded under the same conditions.

ITC

JOX2 WT and mutant proteins were prepared in storage buffer. JA, MeJA, and JA-Ile (Sigma-Aldrich) were dissolved in methanol and diluted with storage buffer to a final concentration of 500 μM. Experiments were performed at 25°C on a MicroCal PEAQ-ITC instrument (Malvern Panalytical). The sample cell containing 400 μl protein (concentration, 50 μM) was titrated with 17 successive injections of 500 μM JA, MeJA, or JA-Ile. Acquired titration curves were fitted with the Origin 7.0 program using the "one set of sites" binding model. The equation of the binding model and the fitting process can be found in the manual "ITC Data Analysis in Origin, Tutorial Guide, Version 7.0, Jan 2004" (https://structbio.vanderbilt.edu/wetlab/private/ITC_Data_Analysis_in_Origin_Tutorial_Guide.pdf). 2OG and Fe(II) were not supplemented in ITC assays because they were co-purified with recombinant JOX2 protein from *E. coli* as shown by the electron density of the crystal structure and the ICP–MS result.

Determination of K_m and V_{max} with a fluorescence-based method

The K_m and V_{max} values of JOX2 WT and mutant proteins were determined with a fluorescence-based method as described previously (McNeill et al., 2005). Each reaction sample contained 10 μg protein, 400 μM 2OG, 1 mM $FeSO_4$, 5 mM sodium L-ascorbate, 5 mM DTT, and JA of various concentrations (0–400 μM). The results were recorded on a microplate reader (SpectraMax i3x, Molecular Devices) with excitation at 340 nm and emission at 420 nm.

Plant growth conditions and *in vivo* assays

Plants were grown on potting soil (Primasta) at 21°C, 70% relative humidity, and 10 h light per day. Pictures were taken from 5-week-old T1 plants and analyzed using PlantCV software. The coding sequences of *JOX2* with different mutations were amplified and cloned into the pENTR vector using Gateway cloning (Invitrogen) and then cloned into the pFast-G02 vector (Shimada et al., 2010) under the control of the 35S promoter. Binary vectors were transformed into *Agrobacterium tumefaciens* strain Agl1, which was used for the transformation of *joxQ* (the quadruple mutant *jox1 jox2 jox3 jox4*) plants using the floral dip method (Clough and Bent, 1998). Transformants were selected based on seed fluorescence to obtain *joxQ 35S:JOX* lines. The presence of the transgene was confirmed by PCR, and its overexpression was confirmed by qRT–PCR as described previously (Caarls et al., 2017).

JA and JA-Ile extraction and quantification

Phytohormones were extracted with cold methanol from leaf material ground in liquid nitrogen (1 ml/100 mg FW). The supernatant (800 μl) was extracted with 800 μl hexane plus 229 μl H_2O, and the lower phase was recovered and dried. Upon reconstitution in 200 μl absolute methanol and centrifugation over a 0.2-μm FTFE filter (Thermo Scientific), analysis was performed using an InfinityLab Poroshell 120 PFP column (1.9 μm, 2.1 × 100 mm; Agilent) and an Agilent G6470 Triple Quad LC–MS instrument (agilent.com). The mobile phase comprised solvent A (10 mM NH_4Ac, 10% [v/v] methanol, 0.5% [v/v] acetic acid in H_2O) and solvent B (10 mM NH_4Ac, 0.5% [v/v] acetic acid in acetonitrile). The gradient was set as follows: 0–0.2 min 100% A; 0.2–3 min to 90% A continued for 0.5 min; 3.5–10 min to 45% A continued for 0.5 min; 10.5–13 min to 5% A continued for 0.5 min; back to 100% A in 0.1 min. The MS conditions were as follows: gas (nitrogen) temperature 260°C; gas flow 5 l/min, nebulizer 45 psi; sheath gas temperature 400°C; sheath gas flow 12 l/min; capillary voltage 3.5 kV; nozzle voltage 0 V. To measure JA and JA-Ile accumulation, we used D5-JA (CDN isotopes, cdnisotopes.com) to calculate recovery; JA and JA-Ile were quantified using standard curves; parent ion/daughter ions were detected in negative mode $[M-H]^-$: JA, 209/59; JA-Ile, 322/130 (fragmentor voltage 125 V, collision energy 16 eV, cell accelerator voltage 4 V).

ACCESSION NUMBERS

The atomic coordinates and structure factors have been deposited in the Protein Data Bank under accession code 6LSV.

SUPPLEMENTAL INFORMATION

Supplemental Information is available at *Molecular Plant Online*.

FUNDING

This research was supported by grants from the National Key Research and Development Program of China (grant no. 2016YFD0300700), the National Natural Science Foundation of China (youth grant, no. 32000859), and the Project for Extramural Scientists of the State Key Laboratory of Agrobiotechnology (project ID: 2020SKLAB6-26). The research of R.S. and G.V.d.A. was financed in part by grants from the Dutch Research Council (NWO).

AUTHOR CONTRIBUTIONS

X.Z., J.L., and Y.-L.P. initiated the project. X.Z., L.Q., and W.S. performed crystallography and *in vitro* experiments. J.E. and R.C.S. performed *in vivo* assays. All authors analyzed the data. X.Z., D.W., R.C.S., G.A., and J.L. wrote the paper.

ACKNOWLEDGMENTS

We thank the staff from the BL18U1 beamline of the National Facility for Protein Science in Shanghai (NFPS) at Shanghai Synchrotron Radiation

Facility for assistance during data collection. We thank Pulu Sun of the University of Amsterdam for her expertise in the determination of JA and JA-Ile contents of plant samples with MS. No conflict of interest declared.

Received: February 20, 2020
Revised: December 20, 2020
Accepted: January 22, 2021
Published: January 27, 2021

REFERENCES

Adams, P.D., Afonine, P.V., Bunkoczi, G., Chen, V.B., Davis, I.W., Echols, N., Headd, J.J., Hung, L.W., Kapral, G.J., Grosse-Kunstleve, R.W., et al. (2010). PHENIX: a comprehensive Python-based system for macromolecular structure solution. Acta Crystallogr. D Biol. Crystallogr. **66**:213–221.

Aik, W.S., Chowdhury, R., Clifton, I.J., et al. (2015). Introduction to Structural Studies on 2-Oxoglutarate-Dependent Oxygenases and Related Enzymes. 2-Oxoglutarate-Dependent Oxygenases (London, UK: Royal Society of Chemistry), pp. 59–94.

Bleijlevens, B., Shivarattan, T., Flashman, E., Yang, Y., Simpson, P.J., Koivisto, P., Sedgwick, B., Schofield, C.J., and Matthews, S.J. (2008). Dynamic states of the DNA repair enzyme AlkB regulate product release. EMBO Rep. **9**:872–877.

Caarls, L., Elberse, J., Awwanah, M., Ludwig, N.R., de Vries, M., Zeilmaker, T., Van Wees, S.C.M., Schuurink, R.C., and Van den Ackerveken, G. (2017). *Arabidopsis* JASMONATE-INDUCED OXYGENASES down-regulate plant immunity by hydroxylation and inactivation of the hormone jasmonic acid. Proc. Natl. Acad. Sci. U S A **114**:6388–6393.

Chen, V.B., Arendall, W.B., 3rd, Headd, J.J., Keedy, D.A., Immormino, R.M., Kapral, G.J., Murray, L.W., Richardson, J.S., and Richardson, D.C. (2010). MolProbity: all-atom structure validation for macromolecular crystallography. Acta Crystallogr. D Biol. Crystallogr. **66**:12–21.

Clough, S.J., and Bent, A.F. (1998). Floral dip: a simplified method for *Agrobacterium*-mediated transformation of *Arabidopsis* thaliana. Plant J. **16**:735–743.

DeLano, W.L. (2002). Pymol Molecular Graphics System (San Carlos, CA: DeLano Scientific).

Devoto, A., Nieto-Rostro, M., Xie, D.X., Ellis, C., Harmston, R., Patrick, E., Davis, J., Sherratt, L., Coleman, M., and Turner, J.G. (2002). COI1 links jasmonate signalling and fertility to the SCF ubiquitin-ligase complex in *Arabidopsis*. Plant J. **32**:457–466.

Emsley, P., and Cowtan, K. (2004). Coot: model-building tools for molecular graphics. Acta Crystallogr. D Biol. Crystallogr. **60**:2126–2132.

Ergel, B., Gill, M.L., Brown, L., Yu, B., Palmer, A.G., 3rd, and Hunt, J.F. (2014). Protein dynamics control the progression and efficiency of the catalytic reaction cycle of the *Escherichia coli* DNA-repair enzyme AlkB. J. Biol. Chem. **289**:29584–29601.

Fernandez-Calvo, P., Chini, A., Fernandez-Barbero, G., Chico, J.M., Gimenez-Ibanez, S., Geerinck, J., Eeckhout, D., Schweizer, F., Godoy, M., Franco-Zorrilla, J.M., et al. (2011). The *Arabidopsis* bHLH transcription factors MYC3 and MYC4 are targets of JAZ repressors and act additively with MYC2 in the activation of jasmonate responses. Plant Cell **23**:701–715.

Fonseca, S., Chini, A., Hamberg, M., Adie, B., Porzel, A., Kramell, R., Miersch, O., Wasternack, C., and Solano, R. (2009). (+)-7-iso-Jasmonoyl-L-isoleucine is the endogenous bioactive jasmonate. Nat. Chem. Biol. **5**:344–350.

Hausinger, R.P. (2015). Biochemical Diversity of 2-Oxoglutarate-Dependent Oxygenases. 2-Oxoglutarate-Dependent Oxygenases (London, UK: Royal Society of Chemistry), pp. 1–58.

Huot, B., Yao, J., Montgomery, B.L., and He, S.Y. (2014). Growth-defense tradeoffs in plants: a balancing act to optimize fitness. Mol. Plant **7**:1267–1287.

Katsir, L., Schilmiller, A.L., Staswick, P.E., He, S.Y., and Howe, G.A. (2008). COI1 is a critical component of a receptor for jasmonate and the bacterial virulence factor coronatine. Proc. Natl. Acad. Sci. U S A **105**:7100–7105.

Kawai, Y., Ono, E., and Mizutani, M. (2014). Evolution and diversity of the 2-oxoglutarate-dependent dioxygenase superfamily in plants. Plant J. **78**:328–343.

Kluza, A., Wojdyla, Z., Mrugala, B., Kurpiewska, K., Porebski, P.J., Niedzialkowska, E., Minor, W., Weiss, M.S., and Borowski, T. (2020). Regioselectivity of hyoscyamine 6beta-hydroxylase-catalysed hydroxylation as revealed by high-resolution structural information and QM/MM calculations. Dalton Trans. **49**:4454–4469.

Liu, A., Ho, R.Y., Que, L., Jr., Ryle, M.J., Phinney, B.S., and Hausinger, R.P. (2001). Alternative reactivity of an alpha-ketoglutarate-dependent iron(II) oxygenase: enzyme self-hydroxylation. J. Am. Chem. Soc. **123**:5126–5127.

Mantri, M., Zhang, Z., McDonough, M.A., and Schofield, C.J. (2012). Autocatalysed oxidative modifications to 2-oxoglutarate dependent oxygenases. FEBS J. **279**:1563–1575.

McNeill, L.A., Bethge, L., Hewitson, K.S., and Schofield, C.J. (2005). A fluorescence-based assay for 2-oxoglutarate-dependent oxygenases. Anal. Biochem. **336**:125–131.

Mitchell, A.J., Dunham, N.P., Martinie, R.J., Bergman, J.A., Pollock, C.J., Hu, K., Allen, B.D., Chang, W.C., Silakov, A., Bollinger, J.M., Jr., et al. (2017). Visualizing the reaction cycle in an iron(II)- and 2-(oxo)-glutarate-dependent hydroxylase. J. Am. Chem. Soc. **139**:13830–13836.

Niu, Y.J., Figueroa, P., and Browse, J. (2011). Characterization of JAZ-interacting bHLH transcription factors that regulate jasmonate responses in *Arabidopsis*. J. Exp. Bot. **62**:2143–2154.

Otwinowski, Z., and Minor, W. (1997). Processing of X-ray diffraction data collected in oscillation mode. Method Enzymol. **276**:307–326.

Peranen, J., Rikkonen, M., Hyvonen, M., and Kaariainen, L. (1996). T7 vectors with modified T7lac promoter for expression of proteins in *Escherichia coli*. Anal. Biochem. **236**:371–373.

Potterton, E., Briggs, P., Turkenburg, M., and Dodson, E. (2003). A graphical user interface to the CCP4 program suite. Acta Crystallogr. D Biol. Crystallogr. **59**:1131–1137.

Ryle, M.J., and Hausinger, R.P. (2002). Non-heme iron oxygenases. Curr. Opin. Chem. Biol. **6**:193–201.

Shimada, T.L., Shimada, T., and Hara-Nishimura, I. (2010). A rapid and non-destructive screenable marker, FAST, for identifying transformed seeds of *Arabidopsis thaliana*. Plant J. **61**:519–528.

Smirnova, E., Marquis, V., Poirier, L., Aubert, Y., Zumsteg, J., Menard, R., Miesch, L., and Heitz, T. (2017). Jasmonic acid oxidase 2 hydroxylates jasmonic acid and represses basal defense and resistance responses against *Botrytis cinerea* infection. Mol. Plant **10**:1159–1173.

Thines, B., Katsir, L., Melotto, M., Niu, Y., Mandaokar, A., Liu, G., Nomura, K., He, S.Y., Howe, G.A., and Browse, J. (2007). JAZ repressor proteins are targets of the SCF(COI1) complex during jasmonate signalling. Nature **448**:661–665.

Wasternack, C., and Strnad, M. (2016). Jasmonate signaling in plant stress responses and development—active and inactive compounds. New Biotechnol. **33**:604–613.

Wilmouth, R.C., Turnbull, J.J., Welford, R.W., Clifton, I.J., Prescott, A.G., and Schofield, C.J. (2002). Structure and mechanism of anthocyanidin synthase from *Arabidopsis thaliana*. Structure **10**:93–103.

Xie, D.X., Feys, B.F., James, S., Nieto-Rostro, M., and Turner, J.G. (1998). COI1: an *Arabidopsis* gene required for jasmonate-regulated defense and fertility. Science **280**:1091–1094.

Yan, J., Yao, R., Chen, L., Li, S., Gu, M., Nan, F., and Xie, D. (2018). Dynamic perception of jasmonates by the F-box protein COI1. Mol. Plant **11**:1237–1247.

Yang, C.G., Yi, C., Duguid, E.M., Sullivan, C.T., Jian, X., Rice, P.A., and He, C. (2008). Crystal structures of DNA/RNA repair enzymes AlkB and ABH2 bound to dsDNA. Nature **452**:961–965.

Zhu, Z., An, F., Feng, Y., Li, P., Xue, L., Mu, A., Jiang, Z., Kim, J.M., To, T.K., Li, W., et al. (2011). Derepression of ethylene-stabilized transcription factors (EIN3/EIL1) mediates jasmonate and ethylene signaling synergy in *Arabidopsis*. Proc. Natl. Acad. Sci. U S A **108**:12539–12544.